energy&fuels

Article

Cite This: *Energy Fuels* 2019, 33, 1882−1891

pubs.acs.org/EF

Microfluidic Study of the Deposition Dynamics of Asphaltene Subfractions Enriched with Island and Archipelago Motifs

Yu-Jiun Lin,[†] Tran Cao,[‡] Martha L. Chacón-Patiño,[§] Steven M. Rowland,[§] Ryan P. Rodgers,[§] Andrew Yen,[‡] and Sibani Lisa Biswal*[,†]

[†]Department of Chemical and Biomolecular Engineering, Rice University, Houston, Texas 77005, United States

[‡]Nalco Champion, An Ecolab Company, Sugar Land, Texas 77478, United States

[§]National High Magnetic Field Laboratory and Future Fuels Institute, Florida State University, Tallahassee, Florida 32310, United States

ABSTRACT: Asphaltene-related flow assurance problems are prevalent in oil production processes and are at the heart of issues such as the plugging of pipelines, the damage of rock formations, and the stabilization of viscous water-in-oil emulsions. A comprehensive understanding of the interfacial behavior of asphaltenes, from a physical−chemical perspective, is required for an accurate design of solutions to these challenges. In this work, we elucidate the deposition dynamics of various asphaltene subfractions in a porous media microfluidic model. Extrography fractions from the interlaboratory sample known as PetroPhase 2017 asphaltenes, reported to be a mixture of abundant island and archipelago motifs, and Wyoming deposit C_7 asphaltenes, known for being island type dominated, are investigated. The deposition rate increases when the compositional ratio archipelago/island motif increases for PetroPhase 2017 derived fractions, whereas Wyoming deposit asphaltenes appear to exhibit stronger aggregation for fractions whose composition is uniformly island type. In general, the deposition rate is consistent with the amount of precipitated asphaltenes. However, the correlation is not merely a linear one and the pore-scale morphology changes even with similar deposition rates. Estimated diffusivity, the relative ratio of convection and diffusion, and fluid flow profiles are used to explain the dynamic growth of the deposit at the pore scale.

1. INTRODUCTION

Asphaltenes are significant contributors to flow assurance challenges because they play a critical role in the stabilization of water-in-oil emulsions and the deposition of solids in petroleum production systems.[1,2] Asphaltenes exist in the oil matrix as relatively stable nanoaggregates. Several works suggest that a combination of intermolecular interactions such as π stacking between aromatic cores, van der Waals interactions between aliphatic moieties, and hydrogen bonding between polarizable functionalities results in strong nanoaggregation.[3−5] Destabilization of these stable nanoaggregates occurs when physicochemical/thermodynamic conditions change, such as the alterations in temperature, pressure, and composition incurred during transportation.[1,6−12]

Crude oil composition also changes in CO_2 or steam injection for enhanced oil recovery (EOR)[13−17] and during the mixing of various crude streams.[18] The attraction between nanoaggregates increases, which results in microaggregation. The combination of destabilization and microaggregation is known as precipitation.[19] During precipitation, asphaltenes tend to either deposit on a surface or form larger particles.[20] This deposition can cause flow assurance problems in pipelines and near-wellbore regions by plugging small-pore throats via mechanical trapping or depositing on rock surfaces, which depicts the complexity of asphaltene deposition to flow assurance.[21,22]

Operationally, asphaltenes are defined as the petroleum species soluble in aromatic solvents such as toluene and benzene and insoluble in *n*-alkanes such as *n*-pentane and *n*-heptane.[6] The specific molecular structure of asphaltene molecules cannot be uniquely defined due to their general classification by solubility. Therefore, asphaltenes are an ultracomplex mixture with possibly over 80000 unique elemental compositions.[23−25] The molecular structure of asphaltenes is proposed to be island, one aromatic core with alkyl side chains, or archipelago, several aromatic cores linked by covalent bridges. Mullins et al. proposed a modified version of the Yen model, concluding that island structures are dominant in petroleum asphaltenes regardless of geological origin and thermal maturity.[26,27] This hypothesis has been supported by Schuler et al., who used atomic force microscopy to access individual molecular structures in virgin and thermally modified asphaltenes. In these studies, hydrogen-deficient ($0.40 < H/C < 0.60$), highly aromatic, and alkyl-deficient island structures were shown to be dominant in both virgin and thermally cracked asphaltenes. Also, few archipelago structures with bridges consisting of one single bond were observed for the first time.[28,29] On the other hand, comprehensive characterization by a novel extrography fractionation and ultrahigh-resolution mass spectrometry demonstrates that asphaltenes comprise a structural continuum of island and archipelago motifs.[30−32] The reason behind the extensive, but incorrect, support of mass spectrometry for the exclusive dominance of island structures is rooted in selective ionization. Moreover, on the basis of asphaltene bulk behavior in mild pyrolysis and thermal cracking, it is hypothesized that

Received: November 2, 2018
Revised: January 3, 2019
Published: February 18, 2019

DOI: 10.1021/acs.energyfuels.8b03835
Energy Fuels 2019, 33, 1882−1891

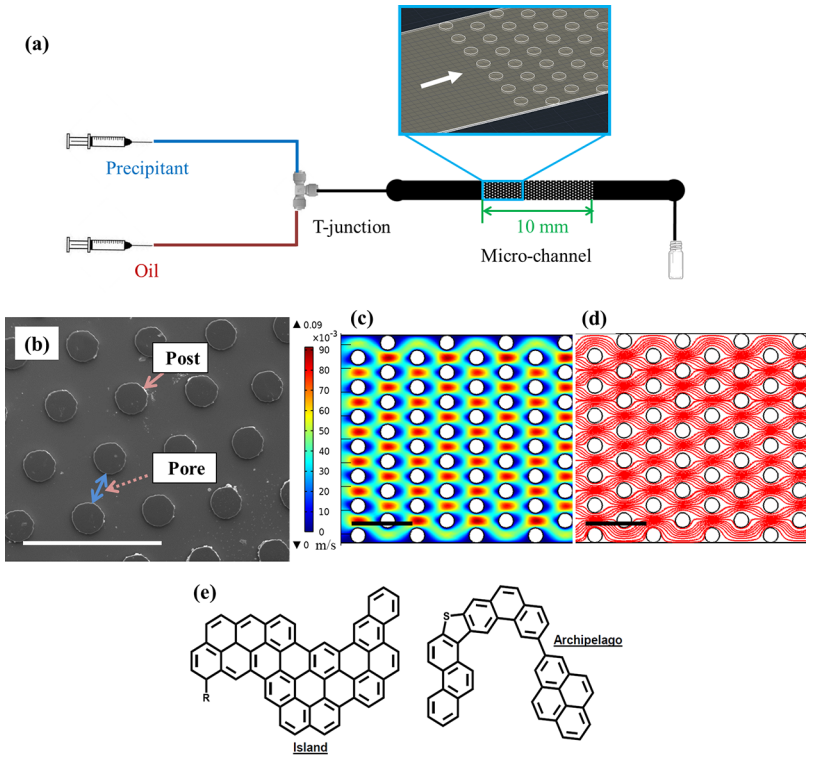

Figure 1. (a) Schematics of the microfluidic system used for studying asphaltene deposition. The blue rectangle is the recording region. (b) SEM image of the porous media design. Scale bars are 500 μm. (c, d) Velocity profile and streamlines of the fluid in the porous media by COMSOL. (e) Schematics of island and archipelago asphaltene molecular structures.

the dominant structure (island or archipelago) is sample dependent.

Sample complexity as well as the dominance of diverse asphaltene structures, island or archipelago, complicates the study of deposition dynamics. To tackle this problem, the scenario of deposition is considered as the particle/colloid deposition in which particles or aggregates are transported by the bulk fluid and adsorb on a surface. Along these lines, two steps for asphaltene deposition are required: first, asphaltene aggregates migrate from the bulk solution to the solid surface by both convection and diffusion based on Brownian motion and fluid flow. When the aggregates are close to the surface, colloidal interactions are dominant in determining if the aggregates would attach on the surface. These interactions mainly depend on the solution chemistry as well as the properties of the aggregate exterior and the surface. The interactions consist of several components, including electrical double layer, van der Waals, and steric forces which are within a short range between the aggregate and the surface.[33]

Asphaltene deposition has been previously examined in capillaries,[10,19,34−40] microfluidic porous media,[9,41−45] and packed bed columns.[46,47] Diffusion is assumed to be a critical factor leading to asphaltene aggregation and deposition.[39,46,48] Microfluidic devices are known for the ease of visualization, the ultralow sample consumption, and the ability to analyze flow processes in great detail and have been used for investigating various oil-related systems such as North American asphaltenes, naphthenic acids, and bitumen.[41,49−53] In this work, we turn to microfluidic micromodels to investigate the effect of variously characterized asphaltene subfractions on deposition dynamics. With the molecular composition known, the deposition behavior is correlated to the molecular structure and chemistry.

2. METHODS AND MATERIALS

2.1. Materials. *n*-heptane (Hep) and toluene (Tol) were reagent grade (purity ≥99%) (Sigma-Aldrich (St. Louis, MO, USA)) and used as received. C_7 asphaltenes used in this study, Wyoming deposit and PetroPhase 2017, were supplied by Nalco Champion and Total. The precipitation, fractionation, and characterization were implemented by the Complex Mixture Group at Florida State University and reported elsewhere.[30−32] The extracting solvents for the extrography fractionation are acetone, heptane, 1/1 heptane/toluene mixture (Hep/Tol), toluene (Tol), 1/1 toluene/tetrahydrofuran mixture (Tol/THF), tetrahydrofuran (THF), and 4/1 tetrahydrofuran/methanol mixture (THF/MeOH).

2.2. Model Oils and Precipitation Tests. Model oils were prepared by slow dissolution of whole C_7 asphaltenes and their subfractions in toluene at a concentration of 0.1 wt %; dissolution was assisted by heating at 90 °C and sonication (40 kHz, ultrasonication bath, Branson) for a minimum of 30 min. Asphaltenes were forced to precipitate out of the model oil by the addition of 80% v/v of *n*-heptane, which was well above the reported instantaneous precipitation point.[9,43] The mass percentage of precipitation of whole samples and subfractions was determined at 80 vol % of heptane. The precipitation measurement was conducted with the centrifugation method reported by Maqbool et al. with a mixing time of 2 min in order to match the flowing time in the microfluidic system used in this study.[54,55]

2.3. Microfluidic Studies. A porous media micromodel was utilized to investigate asphaltene deposition. UV-curable thiolene-based polymer (NOA 81, Norland Optical Adhesive) was chosen as the material of the micromodel with the advantage of high solvent -resistance.[56,57] The detailed fabrication process was described previously.[9] Model oils and *n*-heptane were coinjected by a syringe pump (Harvard Apparatus PHD 2000) and mixed at a T-junction

DOI: 10.1021/acs.energyfuels.8b03835
Energy Fuels 2019, 33, 1882−1891

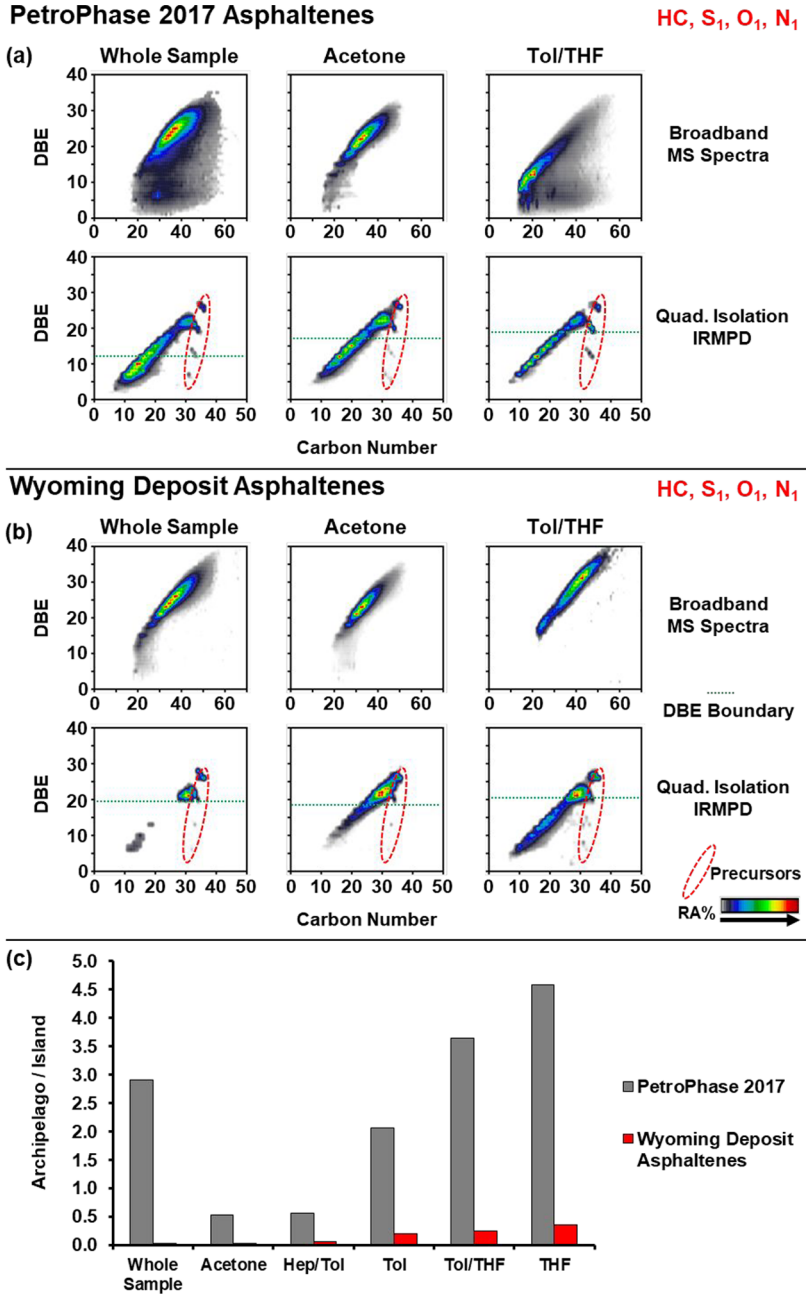

Figure 2. Isoabundance combined color-contoured plots of DBE versus carbon number for HC, S_1, N_1, and O_1 for (a) PetroPhase 2017 and (b) Wyoming asphaltenes. Top rows in (a) and (b) present the broad-band spectra composition; bottom rows in (a) and (b) present the composition for precursor and fragment ions. (c) Relative ratio archipelago/island as a function of fraction for PetroPhase 2017 (gray bars) and Wyoming asphaltenes (red bars). RA denotes relative abundance. Green dotted lines show the DBE boundaries.

(IDEX, MicroTee Assy PEEK-1/16 in) before flowing into the microfluidic device as shown in Figure 1a,b. The length of the porous media is 10 mm, and the permeability of the porous media is around 5.23 Darcy. Both the pore size and the diameter of the post are 125 μm. All experiments were conducted at an ambient temperature of 23 °C. The total flow rate of the fluid mixture was fixed at 60 μL/min (equivalent superficial velocity u = 0.028 m/s). The mass flux of precipitated asphaltenes was approximately ~5 g/(s m^2). The microfluidic device was staged on an inverted microscope (Olympus IX 71), and the visualization of deposition was recorded by a high-speed CMOS camera (Phantom V4.3, Vision Research, Inc.). The microfluidic devices are capable of visualizing particles which are larger than 0.5 μm, which is the limitation of the optical microscope.[19] The images were taken near the entrance of the porous media, assuming the blue rectangle shown in Figure 1a. The experimental images were processed using ImageJ.[58] Images were registered by identifying the location of each post in the porous media. The pixel count associated with asphaltene deposition was determined using Otsu's method.[59] The pixel count was subsequently converted to a coverage area. The velocity profile and streamlines (Figure 1c,d) were obtained by COMSOL version 4.0 with the assumption that the fluid is incompressible. A low-velocity region is found at the front of the post where the streamlines diverge, and a high-velocity region is located on the top and the bottom of the post with the convergence of streamlines. A schematic of island and archipelago asphaltene molecular structures is illustrated in Figure 1e. Asphaltene molecules are made up of polyaromatic hydrocarbons. The island structure, which has been known as a dominant structure of asphaltene, contains a single core of aromatic and naphthenic rings aggregating in a parallel

DOI: 10.1021/acs.energyfuels.8b03835
Energy Fuels 2019, 33, 1882−1891

structure, while the archipelago structure contains multiple small cores which are cross-linked by alkyl bridges.

2.4. Dimensionless Analysis. The Reynolds number is calculated as $\mathrm{Re} = \rho u D_p/(1-\phi)\mu \approx 30$, which is in the laminar region, where $D_p = 6(\text{volume})/(\text{surface area})$ is the equivalent spherical diameter of the obstacle, ρ is the density of the fluid (~720 kg/m^3), μ is the dynamic viscosity of the fluid (~0.4 cP), u is the superficial velocity (0.028 m/s), ϕ is the porosity of the porous media, and A is the cross-sectional area of the microchannel (20 μm × 1800 μm). Deposition can be described in terms of the Péclet number ($\mathrm{Pe} = ud_p/D_{BM}$), where d_p is the diameter of the asphaltene aggregate and D_{BM} is the Brownian diffusivity (m^2/s). This accounts for the relative contributions from convection and diffusion in the presence of different subfractions of asphaltenes.[9,43,60−62] Brownian diffusivity is estimated from the diffusion-limited model with a homogeneous first-order reaction for the deposition derived by Fávero et al.[46] Equation 1 gives the mass balance of asphaltenes in the channel. Equation 2 is obtained by solving eq 1 with the initial condition that $C_A = C_{A0}$ at $x = 0$ and the deposition rate taken as the mass difference between the inlet and the outlet of the microchannel. By substitution of the correlation for mass transfer coefficient reported by Wakao and Thoenes et al., eq 2 can be written as eq 3.[63,64] Then, the particle size can be estimated by the Stokes−Einstein equation ($D_{BM} = k_B T/3\pi\mu d_p$).

$$uA\frac{dC_A}{dx} + k_c a_c A C_A = 0 \tag{1}$$

$$\text{rate}_{dep} = k_c a_c A C_{A0} L \tag{2}$$

$$\text{rate}_{dep} = a_c A C_{A0} L \frac{D_{BM}}{D_p}\frac{1-\phi}{\phi}\mathrm{Re}^{1/2}\mathrm{Sc}^{1/3} \tag{3}$$

where C_A is the concentration of precipitated asphaltenes, x is the distance along the microchannel, $a_c = 6(1-\phi)/\phi$ is the area per volume of the microchannel, k_c is the mass-transfer coefficient, and $\mathrm{Sc} = \mu/\rho D_{BM}$.

3. RESULTS AND DISCUSSION

3.1. Composition and Structure of PetroPhase 2017 and Wyoming Deposit Asphaltenes. Asphaltenes are ultracomplex mixtures that exhibit heterogeneous aggregation, and therefore the characterization by mass spectrometry is biased by selective ionization. Comprehensive MS characterization of asphaltenes is achievable by implementing separation methods that allow sample fractionation based on the aggregation tendency. Therefore, ionization efficiency in techniques such as atmospheric pressure photoionization (APPI) is used. A novel separation method based on aggregation tendency was developed at the National High Magnetic Field Laboratory-Florida State University; it was used to separate PetroPhase 2017 and Wyoming C_7 asphaltenes.[31,32] APPI coupled to Fourier transform ion cyclotron resonance mass spectrometry (FT-ICR MS) provides the elemental composition of thousands of compounds within petroleum samples. APPI is well-suited for the vaporization/ionization of heavy petroleum fractions such as vacuum residues and asphaltenes. Once the sample is transferred to the gas phase, UV photons ionize the gas-phase molecules, which generates mostly molecular ions (radical cations $M^{\bullet+}$) and protonated species $[M + H]^+$. FT-ICR MS allows access to the compositional space of heavy petroleum samples, typically represented by isoabundance color-contoured plots of double bond equivalent (DBE) versus carbon number. To access the molecular structure, the complexity of the sample is typically decreased by the selection of a narrow window of precursor ions through a quadrupole mass filter located before the ICR mass analyzer. Once the precursor ions are transferred to the ICR cell, infrared photons are used to produce fragment ions. A comparison of DBE and carbon number values, between the precursor and the fragment ions, is the basis to discriminate between island and archipelago motifs. This separation method yields a total of eight fractions: acetone, acetonitrile, Hep, Hep/Tol, Tol, Tol/THF, THF, and THF/MeOH. The work presented herein focuses on the whole samples (asphaltenes without fractionation) and their abundant acetone, Hep/Tol, Tol, Tol/THF, and THF fractions.

Figure 2 summarizes the molecular composition and structure for PetroPhase 2017 and Wyoming asphaltenes accessed by positive-ion APPI Fourier transform ion cyclotron resonance (ICR) mass spectrometry and infrared multiphoton dissociation (IRMPD). Figure 2 focuses on the most abundant fractions: acetone and Tol/THF. Figure 2a (top row) presents the isoabundance combined color-contoured plots of DBE versus carbon number for hydrocarbons (class HC, species containing only C and H), and monoheteroatomic classes S_1, O_1, and N_1 (species containing C, H, and one heteroatom) for PetroPhase 2017. The whole PetroPhase 2017 sample exhibits atypical composition, as evidenced by the detection of species with DBE < 15, which is not consistent with the Yen−Mullins model that defines asphaltenes as highly aromatic/alkyl-deficient species. The PetroPhase 2017 acetone fraction, that with the highest ionization efficiency in APPI, is enriched with compounds at the classical asphaltene compositional space, whereas the composition of the Tol/THF fraction, with significantly lower ionization efficiency, shifts to lower atypical DBE values. On the other hand, the molecular composition of whole Wyoming asphaltenes (Figure 2b, top row, left) is typical, enriched with species with DBE > 20 and few carbon atoms in alkyl side chains, as indicated by the narrow range of carbon number for each DBE value. The acetone fraction, also with the highest ionization efficiency, resembles the composition of the whole sample, and the composition of the Tol/THF fraction, with lower ionization efficiency, shifts to higher DBE values with a lower content of alkyl chains.

Figure 2a,b (bottom rows) also presents the fragmentation behavior for whole samples and the fractions acetone and Tol/THF, by presenting the isoabundance combined color-contoured plots of DBE versus carbon number for precursor and fragment ions. The red-dotted ovals highlight the precursor ions that were externally isolated by a mass-resolving quadrupole (m/z ~453−457) and fragmented by infrared multiphoton dissociation inside the ICR mass spectrometer. Both whole samples exhibit opposite fragmentation behavior: fragments derived from PetroPhase 2017 precursors yield abundant fragments with lower carbon number and lower DBE (archipelago motifs) and few island-derived fragments, whereas Wyoming preserves the DBE values of the precursor ions (island motifs). The acetone fractions are enriched with island motifs, whereas the Tol/THF fractions exhibit an increased contribution of archipelago species.

The archipelago−island boundaries were determined for each sample as reported by Chacón-Patiño et al.[31,32] The boundary is a DBE value below which the fragments are considered archipelago-derived. The boundary was calculated as the weighted average DBE for all precursor ions minus the weighted standard deviation. The DBE boundaries for all PetroPhase 2017 fractions range between DBE 13 and 19, whereas the DBE boundaries for all Wyoming asphaltene

DOI: 10.1021/acs.energyfuels.8b03835
Energy Fuels 2019, 33, 1882−1891

fractions range between DBE 18 and 21. Specifically, the DBE boundaries for the whole PetroPhase 2017 sample and its acetone and Tol-THF fractions are 13, 17, and 19. The Wyoming whole sample and its acetone and Tol/THF fractions exhibit DBE boundaries of 19, 18, and 21, respectively. The sum of the relative abundance of the fragments with DBE values below the boundary, divided by the sum of the relative abundance of the fragments with DBE values equal/above the boundary, yields a relative ratio archipelago/island motif, which is presented in Figure 2c. The dominant structural motif for PetroPhase 2017 (whole sample and three of the most abundant fractions) is archipelago (archipelago/island > 1), whereas Wyoming asphaltenes (whole sample and all fractions) are enriched with island motifs (archipelago/island < 1). Importantly, the archipelago/island ratio increases as a function of increasing fraction number for both samples.

3.2. Precipitation Behavior. The mass percentage of precipitation of various subfractions is characterized at 80 vol % of heptane, as shown in Figure 3. The amount of precipitation generally increases with the increase of the ratio of archipelago asphaltenes for PetroPhase 2017 solids, and the whole sample resides in the medium range between island-dominated and archipelago-dominated asphaltenes. Some previous studies have suggested that asphaltene subfractions with higher heteroatom content (more polarizable) exhibit decreased solubility in toluene.[65,66] As reported by Chacón-Patiño et al., Tol/THF and THF extrography fractions from PetroPhase 2017 exhibit higher heteroatom content and lower solubility in toluene.[31] However, no observation of a linear trend is found in the change of the amount of precipitation for Wyoming fractions. The Wyoming whole sample is found to precipitate more than the whole sample of PetroPhase 2017.

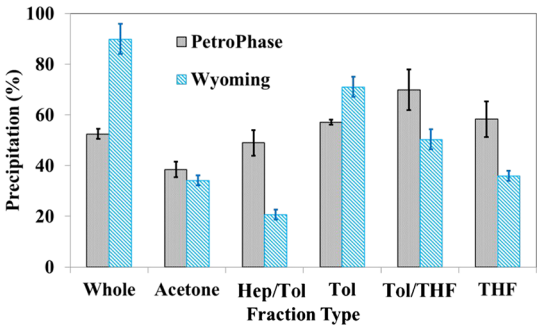

Figure 3. Mass percentage of precipitated asphaltenes, whole samples, and extrography fractions for PetroPhase 2017 (gray bars) and Wyoming deposit asphaltenes (light blue bars).

3.3. Deposition Rate and Morphology of Asphaltene Subfractions. Asphaltene deposition from each fraction was examined, and the representative deposition profiles in porous media are shown in Figure 4 (PetroPhase 2017 asphaltenes) and Figure 5 (Wyoming deposit asphaltenes). In the presence of the precipitant, *n*-heptane, a cone-shaped deposit for the whole PetroPhase 2017 sample is observed at the front of the posts, against the flow direction, as shown in Figure 4a. The cone-shaped deposit can be explained by the velocity and the streamline profiles presented in Figure 1c,d. Higher velocity and assembly of streamlines are found on the top and the bottom of each post, which results in higher local shear stress that prevents asphaltene aggregates from depositing onto surfaces. Conversely, lower velocity and diverging streamlines are obtained at the front of the post, which gives rise to less shear stress and higher chances for asphaltene deposition. The PetroPhase 2017 acetone fraction exhibits shorter deposits with fractal edges (Figure 4b). Cone-shaped deposits are also found for Hep/Tol and toluene fractions (Figure 4c,d), whereas Tol/THF and THF fractions present wide streamlined profiles (Figure 4e,f). In comparison to Figure 4a–d, this wide streamlined shape suggests a softer and smaller particle size since the front tip of the deposit is eroded continuously and small particles can remain on the side of the deposit.

Whole Wyoming deposit asphaltenes exhibit significantly larger formations of the cone-shaped deposit, as illustrated in Figure 5a. Also, the acetone fraction presents a wide streamlined shape of the deposit with fractal edges (Figure 5b). However, as the fraction number increases and the archipelago/island ratio motifs are incremented, the morphology of deposits becomes narrower (Figure 5d) and shorter (Figure 5c–f). Interestingly, the streamline behaviors for the Tol/THF and THF fractions from both asphaltene samples are similar.

The averaged deposition, or deposition coverage (%), as a function of time is quantified by imaging analysis and presented in Figure 6a (PetroPhase 2017) and Figure 6b (Wyoming deposit C_7 asphaltenes). For model oils of PetroPhase 2017 species, the Tol/THF and THF fractions exhibit faster deposition growth in comparison to the other fractions. Interestingly, the growth of the THF fraction follows

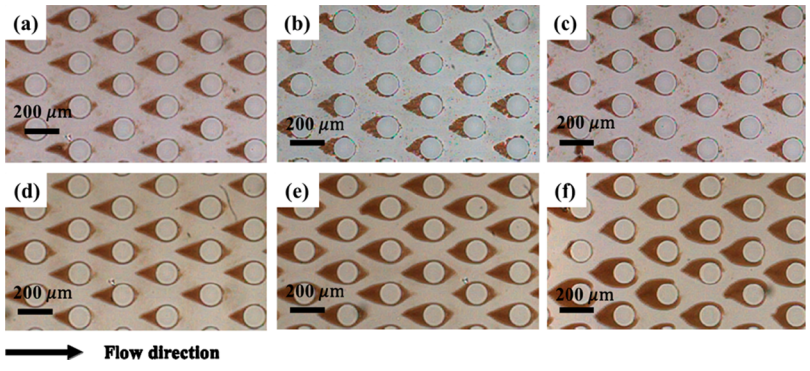

Figure 4. Deposition profile in homogeneous porous media taken at 1800 s near the inlet for the PetroPhase solid: (a) whole PetroPhase 2017 sample and the subfractions that were extracted by (b) acetone, (c) Hep/Tol, (d) Tol, (e) Tol/THF, and (f) THF. Scale bars are 200 μm. Flow direction is from left to right.

DOI: 10.1021/acs.energyfuels.8b03835
Energy Fuels 2019, 33, 1882–1891

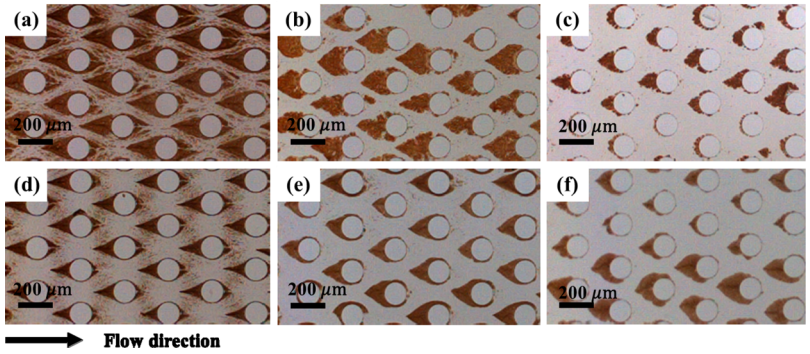

Figure 5. Deposition profile in homogeneous porous media taken at 1800 s near the inlet for Wyoming deposit C_7 asphaltenes: (a) whole sample and the subfractions extracted by (b) acetone, (c) Hep/Tol, (d) Tol (e) Tol/THF, and (f) THF. Scale bars are 200 μm. Flow direction is from left to right.

a fluctuating curve, which suggests that its deposition is a competition between shearing off and growing. Softer asphaltene deposits that produce such fluctuations are also observed when the steric repulsion is enhanced by introducing alkylphenols.[43] Regarding Wyoming deposit, the whole sample and the acetone fraction exhibit a stronger tendency (higher deposition rate) in depositing onto the porous media surface in comparison to the other fractions. The Hep/Tol fraction shows an induction region at the beginning of the deposition process, which suggests that the deposition process is preceded by the formation of a primary layer of asphaltenes on the surface. The deposition rate, obtained from the linear regression of the growth curves presented in Figure 6a,b, is plotted in Figure 6c. Overall, the deposition rate is in a relatively good correlation to the amount of precipitated asphaltenes (C_A), except for the Wyoming acetone fraction, when it is compared with the precipitation results presented in Figure 3.

3.4. Deposition Shape. In regard to Wyoming deposit asphaltenes, it is important to highlight that the shapes of the deposits are different (Figure 5a,b, whole sample versus acetone fraction) even for model oils with similar deposition rates and deposition coverages. It is clear that the correlation between precipitation and deposition is not a simple linear relationship. Therefore, more details about pore-scale visualization and fluid properties are required to properly understand the correlation between deposit morphology and deposition rate/coverage.

There are several factors that are known to affect the rate of deposition for the two different types of molecular structures, including possible increased steric repulsion from alkyl substituents, different heteroatom contents affecting solubility in solvents, and stabilizing effects from island motifs on archipelago fractions. The deposition rate of PetroPhase fractions generally increases as a function of an increase in the ratio of archipelago/island motifs. First of all, this deposition increment is possibly caused by the higher content of alkyl substituents present in archipelago asphaltenes, which results in greater steric repulsion and smaller aggregates. A minimum deposition rate was found to be dependent on the particle size. Specifically, when the particle size is below a critical size of approximately 1 μm, thermal motion is able to keep the deposits suspended. However, for aggregates that are larger than the critical suspended size, convection results in more impact with the porous media. This results in a lower deposition rate for larger sub-micrometer asphaltene aggregates.[67,68] Additionally, the increase in the steric repulsion between asphaltenes results in smaller aggregates and higher deposition rate in some cases.[43] Second, as discussed in section 3.2, Tol/THF and THF extrography fractions from PetroPhase 2017 exhibit higher heteroatom content and lower solubility in toluene.[31] These characteristics could lead to a stronger deposition in the microfluidic device used in this work.[66,69] However, higher heteroatom content and lower solubility suggest a lack of correlation between the size of asphaltene aggregates and the rate of deposition. Third, it is important to highlight that the deposition rate of the whole PetroPhase 2017 sample falls between that of the acetone fraction (island dominated) and that of the toluene fraction (archipelago dominated), which suggests that island species act as stabilizers for archipelago/polarizable structures, leading to a decrease in the deposition rate for the whole sample. Kilpatrick, Fogler et al. have also pointed out cooperative stabilization between asphaltene subfractions obtained by differential precipitation in Hep/Tol. In their studies, asphaltene subfractions with higher solubility in Hep/Tol (lower heteroatom content) were shown to stabilize "polar" (higher heteroatom content) asphaltene subfractions.[65,66]

Regarding Wyoming deposit asphaltene species, there are no clear trends for deposition rate and precipitation. As previously reported, the dominant motif in whole Wyoming deposit asphaltenes is island (<90%). Among the extrography fractions, acetone, the most island-enriched virgin sample ever observed by the group at Florida State University, exhibits the highest deposition rate in the microfluidic system. These results suggest that island-enriched asphaltenes can exhibit a higher deposition rate when the composition is highly uniform/island type. Interestingly, Hep/Tol, Tol, Tol/THF, and THF fractions present a lower deposition rate in the microfluidic system in comparison with acetone. These results are puzzling, since the later fractions, particularly Tol and Tol/THF, exhibit the highest DBE and the lowest content of alkyl substituents and therefore according to the Yen–Mullins model should exhibit stronger aggregation/deposition.

The diffusivity of each fraction can be determined by fitting the deposition rate and the amount of precipitated asphaltenes in the diffusion-limited model (eq 3). The diffusivity of whole asphaltenes and their subfractions are given in Table 1. Generally, the calculated diffusivities of PetroPhase 2017 species are smaller than those of Wyoming deposit fractions. It is important to keep in mind that the Stokes–Einstein equation takes into account the equivalent particle diameter

DOI: 10.1021/acs.energyfuels.8b03835
Energy Fuels 2019, 33, 1882–1891

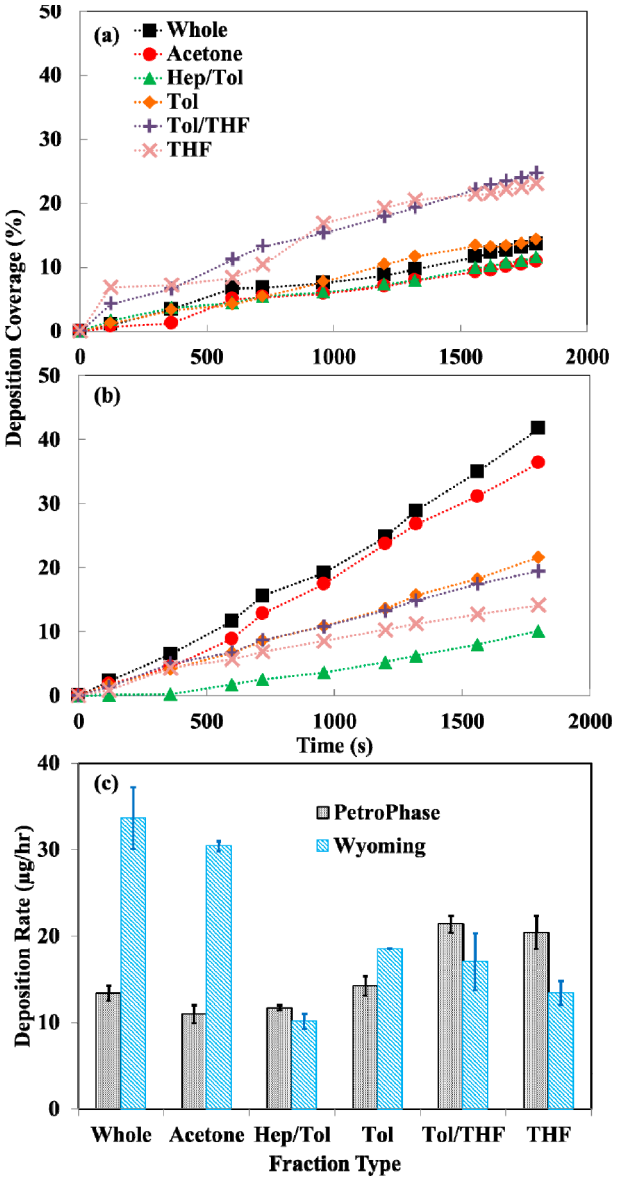

Figure 6. Deposition curves for model oils comprised of whole asphaltene samples (black ■), acetone (red ●), Hep/Tol (green ▲), Tol (orange ◆), Tol/THF (purple +), and THF (pink ×) fractions for (a) PetroPhase 2017 and (b) Wyoming deposit. (c) Deposition rate obtained from the linear regression of the curves presented in Figure 6a and Figure 6b.

and the Péclet number (Pe = ud_p/D_{BM}). It is used to determine the relative contributions of convection and diffusion, since the determining factor in deposition with submicron aggregates is assumed to be diffusion. In this regard, when the contribution of convection increases, the deposition rate decreases.[67] Regarding PetroPhase 2017 fractions, the equivalent particle diameter decreases as a function of increasing the archipelago/island motif ratios. We hypothesize that this decrease is the result of the steric repulsion that arises from greater alkyl chain content.

The equivalent particle diameter for Wyoming fractions is relatively smaller. Since the structure of Wyoming species is dominated by island motifs (above 90%), these results suggest that this smaller size might be caused by the stabilization of island asphaltenes by $\pi-\pi$ interactions from the aromatic solvent (toluene). However, introducing more archipelago asphaltenes into the system might result in both stronger and weaker aggregation for larger and smaller aggregates. The reason is still unclear and requires more investigations on the interactions between asphaltene molecules. The estimated Péclet number is utilized to explain the pore-scale visualization in the following section.

3.5. Pore-Scale Visualization of the Deposition Profile for Various Asphaltene Subfraction. The dynamics of the pore-scale deposition growth is illustrated in Figure 7 taken at 1800 s. From previous studies, asphaltenes produce cone-shaped deposits at the front of the post when Pe increases and create streamlined-shaped deposits when Pe decreases.[9] Softer deposits are also reported when steric repulsion is enhanced.[43] Whole PetroPhase 2017 and Wyoming samples exhibit relatively higher Pe and produce cone-shaped deposits. For both whole samples, the dynamic growth curves are similar; it is clear that the deposit grows from a smaller cone into a larger cone. However, PetroPhase 2017 and Wyoming deposit whole samples, with Péclet numbers equal to 1.1×10^3 and 3.4×10^2, respectively, exhibit a slight difference in the deposition pattern: Wyoming asphaltenes show deposition at the rear of the post, which suggests that a smaller Péclet number results in higher possibility for aggregates to diffuse and deposit. This has also been suggested to be caused by the circulation of the flow at the rear of the post found in numerical simulations by Kusaka et al.[61] The cone-shaped deposits observed in Figure 7 can also be explained by the velocity profile and the pressure, as illustrated in Figure 8. High-velocity regions are distributed on the top and the bottom of the post, resulting in strong shear stress that prevents aggregate deposition. Also, the pressure changes significantly at the locations with $x = -25$ μm and $y = \pm 50$ μm. This discrepancy of pressure forces the aggregates to migrate. For both acetone fractions, Pe values are smaller in comparison to the whole samples; these fractions exhibit fractal edges as well as streamlined dynamic growth curves (Figure 7b,e). The Wyoming acetone fraction (Figure 7e) shows a wide streamlined shape with a significantly smaller Pe, which is

Table 1. Calculated Properties of PetroPhase and Wyoming Fractions

	whole	acetone	Hep/Tol	Tol	Tol/THF	THF
			PetroPhase			
D_{BM} (10^{12} m^2 s^{-1})	5.14	6.08	4.65	4.96	6.75	8.28
d_p (nm)	201	170	223	209	153	125
Pe	1.1×10^3	7.8×10^2	1.3×10^3	1.2×10^3	6.3×10^2	4.5×10^2
			Wyoming			
D_{BM} (10^{12} m^2 s^{-1})	9.15	33.62	13.74	5.32	7.87	9.08
d_p (nm)	113	31	75	195	132	114
Pe	3.4×10^2	2.5×10^1	1.5×10^2	1.0×10^3	4.7×10^2	3.5×10^2

DOI: 10.1021/acs.energyfuels.8b03835
Energy Fuels 2019, 33, 1882−1891

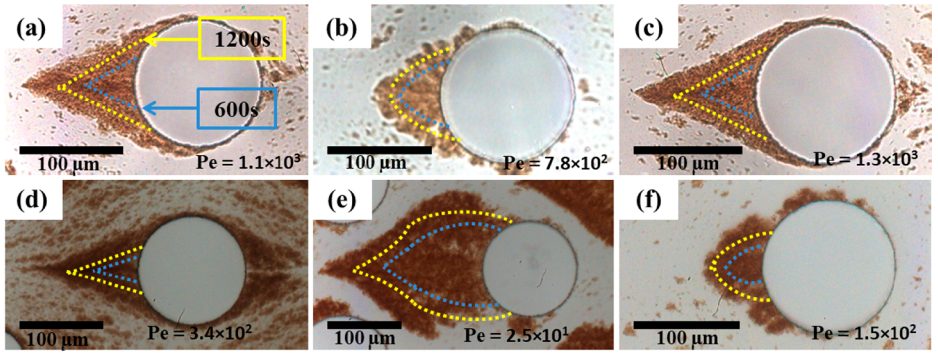

Figure 7. Schematic dynamics of asphaltene deposition growth for PetroPhase 2017 (a–c) and Wyoming deposit asphaltenes (d–f) taken at 1800 s: whole samples (a, d); acetone fractions (b, e), and Hep/Tol fractions (c, f). Dotted blue lines correspond to 600 s, and dotted yellow lines correspond to 1200 s. The scale bar is 100 μm. Péclet number: (a) 1.1×10^3; (b) 7.8×10^2; (c) 1.3×10^3; (d) 3.4×10^2; (e) 2.5×10^1; (f) 1.5×10^2.

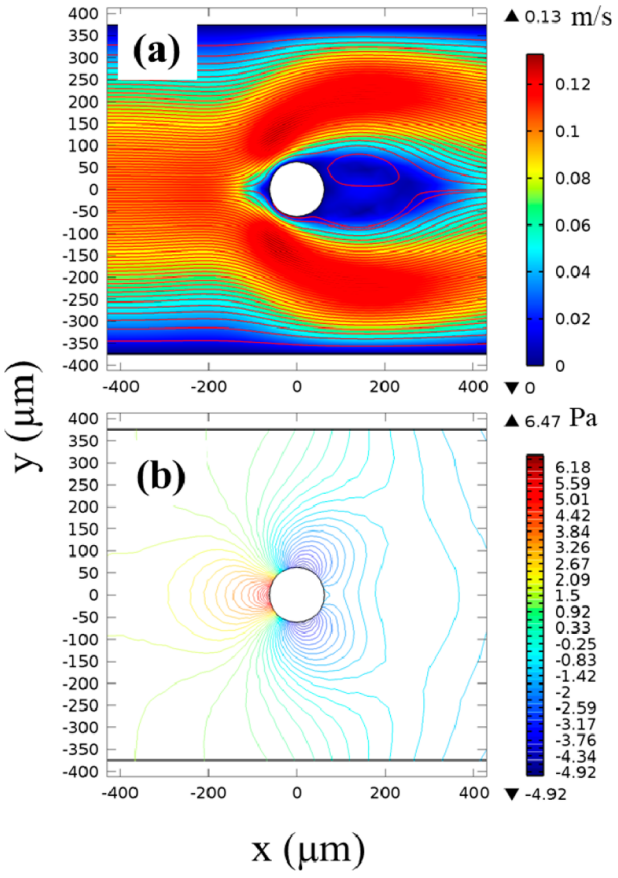

Figure 8. Velocity and pressure profiles around a representative single post.

consistent with the work by Lin et al., who found that small Pe values are strongly correlated to streamlined deposits because the aggregates tend to deposit without being carried/transported by the fluid flow.[43] Interestingly, when the Hep/Tol fractions are compared (Figure 7c,f), Wyoming deposit asphaltenes exhibits a Pe 1 order of magnitude smaller than that of PetroPhase 2017 species. This decrease translates into a change of the deposit shape, from sharp conelike (higher Pe) to fractal deposit (lower Pe). Other materials such as latex particles also exhibit similar trends: smaller Péclet numbers correlate with fractal deposits, whereas larger values are associated with cone-shaped/more uniform deposits.[61] The dynamic growth curve for Wyoming Hep/Tol fraction (Figure 7f) also suggests that a system with a lower Pe tends to produce deposits that grow in a streamlined pattern. No observation of the deposit at the rear of the post in Figure 7e,f even with lower Pe could result from the smaller amount of precipitated particles, causing a lower deposition tendency.

4. CONCLUSIONS

Microfluidic devices offer a well-controlled platform for highly surface sensitive and limited materials. The visualizing capability also provides insightful information on the fundamental investigation of the asphaltene deposition mechanism. Two asphaltene solids are fractionated, and the chemical structure is characterized. These mass fraction samples are very limited, and therefore microfluidic devices can be used to study their deposition dynamics. For PetroPhase 2017 fractions, which mainly consist of archipelago species, the deposition correlates well with the archipelago to island asphaltene ratio. Also, the deposition rate of the whole sample falls between island-type and archipelago-type asphaltenes, which suggests that the island-dominated asphaltenes are capable of stabilizing the archipelago-dominated fractions. Also, the observed streamlined shape and fluctuating deposition growth suggest a possible softer formation for archipelago-dominated fractions. However, for the Wyoming fractions, which mainly consist of island species, deposition is not well correlated to species ratio. For the Wyoming sample, the acetone fraction has the smallest Pe and the highest deposition rate. These results could arouse people to consider modifying mitigation methods when the type of asphaltene is known, especially for the design of the asphaltene deposition inhibitors. On the basis of the results shown in this study, island-type asphaltenes could be the inhibitors or stabilizers for archipelago asphaltene dominated oils. For island asphaltene dominated oil, an increased content of archipelago-type asphaltenes could potentially reduce the deposition tendency.

AUTHOR INFORMATION

Corresponding Author

*E-mail for S.L.B.: biswal@rice.edu.

ORCID

Yu-Jiun Lin: 0000-0002-0655-9580
Ryan P. Rodgers: 0000-0003-1302-2850
Sibani Lisa Biswal: 0000-0002-0610-835X

DOI: 10.1021/acs.energyfuels.8b03835
Energy Fuels 2019, 33, 1882–1891

Notes

The authors declare no competing financial interest.

■ ACKNOWLEDGMENTS

We thank Patrick Gilliam and Zhuqing Zhang for their technical assistance and Nalco Champion for financial support.

■ REFERENCES

(1) Creek, J. L. Freedom of Action in the State of Asphaltenes: Escape from Conventional Wisdom. *Energy Fuels* **2005**, *19* (4), 1212−1224.

(2) Lin, Y.-J.; Barman, S.; He, P.; Zhang, Z.; Christopher, G. F.; Biswal, S. L. Combined Interfacial Shear Rheology and Microstructure Visualization of Asphaltenes at Air-Water and Oil-Water Interfaces. *J. Rheol.* **2018**, *62* (1), 1−10.

(3) Gray, M. R.; Tykwinski, R. R.; Stryker, J. M.; Tan, X. Supramolecular Assembly Model for Aggregation of Petroleum Asphaltenes. *Energy Fuels* **2011**, *25* (7), 3125−3134.

(4) Chacón-Patiño, M. L.; Blanco-Tirado, C.; Orrego-Ruiz, J. A.; Gómez-Escudero, A.; Combariza, M. Y. High Resolution Mass Spectrometric View of Asphaltene−SiO_2 Interactions. *Energy Fuels* **2015**, *29* (3), 1323−1331.

(5) Murgich, J. INTERMOLECULAR FORCES IN AGGREGATES OF ASPHALTENES AND RESINS. *Pet. Sci. Technol.* **2002**, *20* (9−10), 983−997.

(6) Vargas, F. M.; Gonzalez, D. L.; Creek, J. L.; Wang, J.; Buckley, J.; Hirasaki, G. J.; Chapman, W. G. Development of a General Method for Modeling Asphaltene Stability. *Energy Fuels* **2009**, *23* (3), 1147−1154.

(7) Chaisoontornyotin, W.; Haji-Akbari, N.; Fogler, H. S.; Hoepfner, M. P. Combined Asphaltene Aggregation and Deposition Investigation. *Energy Fuels* **2016**, *30* (3), 1979−1986.

(8) Chaisoontornyotin, W.; Bingham, A. W.; Hoepfner, M. P. Reversibility of Asphaltene Precipitation Using Temperature-Induced Aggregation. *Energy Fuels* **2017**, *31*, 3392.

(9) Lin, Y.-J.; He, P.; Tavakkoli, M.; Mathew, N. T.; Fatt, Y. Y.; Chai, J. C.; Goharzadeh, A.; Vargas, F. M.; Biswal, S. L. Examining Asphaltene Solubility on Deposition in Model Porous Media. *Langmuir* **2016**, *32* (34), 8729−8734.

(10) Zhuang, Y.; Goharzadeh, A.; Lin, Y. J.; Yap, Y. F.; Chai, J. C.; Mathew, N.; Vargas, F.; Biswal, S. L. Three Dimensional Measurements of Asphaltene Deposition in a Transparent Micro-Channel. *J. Pet. Sci. Eng.* **2016**, *145*, 77−82.

(11) Zhuang, Y.; Goharzadeh, A.; Lin, Y. J.; Yap, Y. F.; Chai, J. C.; Mathew, N.; Vargas, F.; Biswal, S. L. Experimental Study of Asphaltene Deposition in Transparent Microchannels Using Light Absorption Method. *J. Dispersion Sci. Technol.* **2018**, *39*, 744.

(12) Lin, Y.-J.; Perrard, A.; Biswal, S. L.; Hill, R. M.; Trabelsi, S. Microfluidic Investigation of Asphaltenes-Stabilized Water-in-Oil Emulsions. *Energy Fuels* **2018**, *32* (4), 4903−4910.

(13) Verdier, S.; Carrier, H.; Andersen, S. I.; Daridon, J.-L. Study of Pressure and Temperature Effects on Asphaltene Stability in Presence of CO_2. *Energy Fuels* **2006**, *20* (4), 1584−1590.

(14) Novosad, Z.; Costain, T. G. *Experimental and Modeling Studies of Asphaltene Equilibria for a Reservoir Under CO2 Injection*; Society of Petroleum Engineers, 1990. DOI: 10.2118/20530-MS.

(15) Sie, C.-Y.; Nguyen, B.; Verlaan, M.; Castellanos-Diaz, O.; Adiaheno, K.; Nguyen, Q. P. Viscous Oil Recovery and In Situ Deasphalting in Fractured Reservoirs: Part 1. The Effect of Solvent Injection Rate. *Energy Fuels* **2018**, *32* (1), 360−372.

(16) Tang, B.; Anand, N.; Nguyen, B.; Sie, C.; Verlaan, M.; Díaz, O. C.; Nguyen, Q. P. *Experimental and Theoretical Study of Operating Pressure and Capillary Pressure on Vapor Oil Gravity Drainage VOGD in Fractured Reservoirs*. In SPE Improved Oil Recovery Conference; Society of Petroleum Engineers: Tulsa, Oklahoma, USA, 2018. DOI: 10.2118/190251-MS.

(17) Anand, N.; Tang, B. C.; Nguyen, B.; Sie, C.; Verlaan, M.; Castellanos-Diaz, O.; Nguyen, Q. P. *Experimental and Theoretical Study of Rate, Temperature and Solvent-Type Effects on Vapor Oil Gravity Drainage VOGD in Fractured Reservoirs*. In SPE EOR Conference at Oil and Gas West Asia; Society of Petroleum Engineers: Muscat, Oman, 2018. DOI: 10.2118/190350-MS.

(18) Pazuki, G. R.; Nikookar, M. A Modified Flory-Huggins Model for Prediction of Asphaltenes Precipitation in Crude Oil. *Fuel* **2006**, *85* (7−8), 1083−1086.

(19) Hoepfner, M. P.; Limsakoune, V.; Chuenmeechao, V.; Maqbool, T.; Fogler, H. S. A Fundamental Study of Asphaltene Deposition. *Energy Fuels* **2013**, *27* (2), 725−735.

(20) Vargas, F. M.; Creek, J. L.; Chapman, W. G. On the Development of an Asphaltene Deposition Simulator. *Energy Fuels* **2010**, *24* (4), 2294−2299.

(21) Gruesbeck, C.; Collins, R. E. Entrainment and Deposition of Fine Particles in Porous Media. *SPEJ, Soc. Pet. Eng. J.* **1982**, *22* (06), 847−856.

(22) Wang, S.; Civan, F. *Productivity Decline of Vertical and Horizontal Wells by Asphaltene Deposition in Petroleum Reservoirs*; Society of Petroleum Engineers, 2001. DOI: 10.2118/64991-MS.

(23) McKenna, A. M.; Marshall, A. G.; Rodgers, R. P. Heavy Petroleum Composition. 4. Asphaltene Compositional Space. *Energy Fuels* **2013**, *27* (3), 1257−1267.

(24) Witt, M.; Godejohann, M.; Oltmanns, S.; Moir, M.; Rogel, E. Characterization of Asphaltenes Precipitated at Different Solvent Power Conditions Using Atmospheric Pressure Photoionization (APPI) and Laser Desorption Ionization (LDI) Coupled to Fourier Transform Ion Cyclotron Resonance Mass Spectrometry (FT-ICR MS). *Energy Fuels* **2018**, *32* (3), 2653−2660.

(25) Purcell, J. M.; Merdrignac, I.; Rodgers, R. P.; Marshall, A. G.; Gauthier, T.; Guibard, I. Stepwise Structural Characterization of Asphaltenes during Deep Hydroconversion Processes Determined by Atmospheric Pressure Photoionization (APPI) Fourier Transform Ion Cyclotron Resonance (FT-ICR) Mass Spectrometry †. *Energy Fuels* **2010**, *24* (4), 2257−2265.

(26) Mullins, O. C. The Modified Yen Model †. *Energy Fuels* **2010**, *24* (4), 2179−2207.

(27) Mullins, O. C.; Sabbah, H.; Eyssautier, J.; Pomerantz, A. E.; Barré, L.; Andrews, A. B.; Ruiz-Morales, Y.; Mostowfi, F.; McFarlane, R.; Goual, L.; et al. Advances in Asphaltene Science and the Yen−Mullins Model. *Energy Fuels* **2012**, *26* (7), 3986−4003.

(28) Schuler, B.; Meyer, G.; Peña, D.; Mullins, O. C.; Gross, L. Unraveling the Molecular Structures of Asphaltenes by Atomic Force Microscopy. *J. Am. Chem. Soc.* **2015**, *137* (31), 9870−9876.

(29) Schuler, B.; Fatayer, S.; Meyer, G.; Rogel, E.; Moir, M.; Zhang, Y.; Harper, M. R.; Pomerantz, A. E.; Bake, K. D.; Witt, M.; et al. Heavy Oil Based Mixtures of Different Origins and Treatments Studied by Atomic Force Microscopy. *Energy Fuels* **2017**, *31* (7), 6856−6861.

(30) Chacón-Patiño, M. L.; Rowland, S. M.; Rodgers, R. P. Advances in Asphaltene Petroleomics. Part 1: Asphaltenes Are Composed of Abundant Island and Archipelago Structural Motifs. *Energy Fuels* **2017**, *31* (12), 13509−13518.

(31) Chacón-Patiño, M. L.; Rowland, S. M.; Rodgers, R. P. Advances in Asphaltene Petroleomics. Part 2: Selective Separation Method That Reveals Fractions Enriched in Island and Archipelago Structural Motifs by Mass Spectrometry. *Energy Fuels* **2018**, *32* (1), 314−328.

(32) Chacón-Patiño, M. L.; Rowland, S. M.; Rodgers, R. P. Advances in Asphaltene Petroleomics. Part 3. Dominance of Island or Archipelago Structural Motif Is Sample Dependent. *Energy Fuels* **2018**, *32*, 9106.

(33) *Particle Deposition and Aggregation: Measurement, Modelling and Simulation*; Elimelech, M., Ed.; Butterworth-Heinemann: Oxford, 1998; Colloid and surface engineering series

(34) Wang, J.; Buckley, J. S.; Creek, J. L. Asphaltene Deposition on Metallic Surfaces. *J. Dispersion Sci. Technol.* **2004**, *25* (3), 287−298.

(35) Nabzar, L.; Aguiléra, M. E. The Colloidal Approach. A Promising Route for Asphaltene Deposition Modelling. *Oil Gas Sci. Technol.* **2008**, *63* (1), 21−35.

DOI: 10.1021/acs.energyfuels.8b03835
Energy Fuels 2019, 33, 1882−1891

(36) Hashmi, S. M.; Loewenberg, M.; Firoozabadi, A. Colloidal Asphaltene Deposition in Laminar Pipe Flow: Flow Rate and Parametric Effects. *Phys. Fluids* **2015**, *27* (8), 083302.
(37) Lawal, K. A.; Crawshaw, J. P.; Boek, E. S.; Vesovic, V. Experimental Investigation of Asphaltene Deposition in Capillary Flow. *Energy Fuels* **2012**, *26* (4), 2145−2153.
(38) Boek, E. S.; Ladva, H. K.; Crawshaw, J. P.; Padding, J. T. Deposition of Colloidal Asphaltene in Capillary Flow: Experiments and Mesoscopic Simulation. *Energy Fuels* **2008**, *22* (2), 805−813.
(39) Chaisoontornyotin, W.; Haji-Akbari, N.; Fogler, H. S.; Hoepfner, M. P. Combined Asphaltene Aggregation and Deposition Investigation. *Energy Fuels* **2016**, *30* (3), 1979−1986.
(40) Li, X.; Guo, Y.; Sun, Q.; Lan, W.; Liu, A.; Guo, X. Experimental Study for the Impacts of Flow Rate and Concentration of Asphaltene Precipitant on Dynamic Asphaltene Deposition in Microcapillary Medium. *J. Pet. Sci. Eng.* **2018**, *162*, 333−340.
(41) Hu, C.; Morris, J. E.; Hartman, R. L. Microfluidic Investigation of the Deposition of Asphaltenes in Porous Media. *Lab Chip* **2014**, *14* (12), 2014−2022.
(42) Hu, C.; Yen, A.; Joshi, N.; Hartman, R. L. Packed-Bed Microreactors for Understanding of the Dissolution Kinetics and Mechanisms of Asphaltenes in Xylenes. *Chem. Eng. Sci.* **2016**, *140*, 144−152.
(43) Lin, Y.-J.; He, P.; Tavakkoli, M.; Mathew, N. T.; Fatt, Y. Y.; Chai, J. C.; Goharzadeh, A.; Vargas, F. M.; Biswal, S. L. Characterizing Asphaltene Deposition in the Presence of Chemical Dispersants in Porous Media Micromodels. *Energy Fuels* **2017**, *31* (11), 11660−11668.
(44) Keshmiri, K.; Huang, H.; Nazemifard, N. Microfluidic Platform to Evaluate Asphaltene Deposition during Solvent-Based Extraction of Bitumen. *Fuel* **2019**, *239*, 841−851.
(45) Xu, L.; Abedini, A.; Qi, Z.; Kim, M.; Guerrero, A.; Sinton, D. Pore-Scale Analysis of Steam-Solvent Coinjection: Azeotropic Temperature, Dilution and Asphaltene Deposition. *Fuel* **2018**, *220*, 151−158.
(46) Vilas Bôas Fávero, C.; Hanpan, A.; Phichphimok, P.; Binabdullah, K.; Fogler, H. S. Mechanistic Investigation of Asphaltene Deposition. *Energy Fuels* **2016**, *30* (11), 8915−8921.
(47) Kuang, J.; Tavakkoli, M.; Yarbrough, J.; Wang, J.; Jain, S.; Ashtekar, S.; Abdallah, D. S.; Punnapala, S.; Vargas, F. M. Investigation of Asphaltene Deposition at High Temperature and under Dynamic Conditions. *Energy Fuels* **2018**, *32*, 12405.
(48) Chaisoontornyotin, W.; Zhang, J.; Ng, S.; Hoepfner, M. P. Rapid Heterogeneous Asphaltene Precipitation with Dispersed Solids. *Energy Fuels* **2018**, *32* (7), 7458−7466.
(49) Kim, M.; Sell, A.; Sinton, D. Aquifer-on-a-Chip: Understanding Pore-Scale Salt Precipitation Dynamics during CO2 Sequestration. *Lab Chip* **2013**, *13* (13), 2508.
(50) Bowden, S. A.; Wilson, R.; Parnell, J.; Cooper, J. M. Determination of the Asphaltene and Carboxylic Acid Content of a Heavy Oil Using a Microfluidic Device. *Lab Chip* **2009**, *9* (6), 828−832.
(51) Qi, Z.; Abedini, A.; Sharbatian, A.; Pang, Y.; Guerrero, A.; Sinton, D. Asphaltene Deposition during Bitumen Extraction with Natural Gas Condensate and Naphtha. *Energy Fuels* **2018**, *32* (2), 1433−1439.
(52) Sharbatian, A.; Abedini, A.; Qi, Z.; Sinton, D. Full Characterization of CO_2 − Oil Properties On-Chip: Solubility, Diffusivity, Extraction Pressure, Miscibility, and Contact Angle. *Anal. Chem.* **2018**, *90* (4), 2461−2467.
(53) Squires, T. M.; Quake, S. R. Microfluidics: Fluid Physics at the Nanoliter Scale. *Rev. Mod. Phys.* **2005**, *77* (3), 977−1026.
(54) Maqbool, T.; Srikiratiwong, P.; Fogler, H. S. Effect of Temperature on the Precipitation Kinetics of Asphaltenes. *Energy Fuels* **2011**, *25* (2), 694−700.
(55) Vilas Bôas FáVero, C.; Maqbool, T.; Hoepfner, M.; Haji-Akbari, N.; Fogler, H. S. Revisiting the Flocculation Kinetics of Destabilized Asphaltenes. *Adv. Colloid Interface Sci.* **2017**, *244*, 267−280.
(56) Wägli, P.; Homsy, A.; de Rooij, N. F. Norland Optical Adhesive (NOA81) Microchannels with Adjustable Wetting Behavior and High Chemical Resistance against a Range of Mid-Infrared-Transparent Organic Solvents. *Sens. Actuators, B* **2011**, *156* (2), 994−1001.
(57) Hung, L.-H.; Lin, R.; Lee, A. P. Rapid Microfabrication of Solvent-Resistant Biocompatible Microfluidic Devices. *Lab Chip* **2008**, *8* (6), 983−987.
(58) Schneider, C. A.; Rasband, W. S.; Eliceiri, K. W. NIH Image to ImageJ: 25 Years of Image Analysis. *Nat. Methods* **2012**, *9* (7), 671−675.
(59) Otsu, N. A Threshold Selection Method from Gray-Level Histograms. *IEEE Trans. Syst. Man Cybern.* **1979**, *9* (1), 62−66.
(60) Adamczyk, Z.; Van De Ven, T. G. Deposition of Brownian Particles onto Cylindrical Collectors. *J. Colloid Interface Sci.* **1981**, *84* (2), 497−518.
(61) Kusaka, Y.; Duval, J. F. L.; Adachi, Y. Morphology and Breaking of Latex Particle Deposits at a Cylindrical Collector in a Microfluidic Chamber. *Environ. Sci. Technol.* **2010**, *44* (24), 9413−9418.
(62) Robert de Saint Vincent, M.; Abkarian, M.; Tabuteau, H. Dynamics of Colloid Accumulation under Flow over Porous Obstacles. *Soft Matter* **2016**, *12* (4), 1041−1050.
(63) Wakao, N.; Funazkri, T. Effect of Fluid Dispersion Coefficients on Particle-to-Fluid Mass Transfer Coefficients in Packed Beds. *Chem. Eng. Sci.* **1978**, *33* (10), 1375−1384.
(64) Thoenes, D.; Kramers, H. Mass Transfer from Spheres in Various Regular Packings to a Flowing Fluid. *Chem. Eng. Sci.* **1958**, *8* (3−4), 271−283.
(65) Wattana, P.; Fogler, H. S.; Yen, A.; Carmen Garcìa, M. D.; Carbognani, L. Characterization of Polarity-Based Asphaltene Subfractions. *Energy Fuels* **2005**, *19* (1), 101−110.
(66) Gawrys, K. L.; Matthew Spiecker, P.; Kilpatrick, P. K. The Role of Asphaltene Solubility and Chemical Composition on Asphaltene Aggregation. *Pet. Sci. Technol.* **2003**, *21* (3−4), 461−489.
(67) Yao, K.-M.; Habibian, M. T.; O'Melia, C. R. Water and Waste Water Filtration. Concepts and Applications. *Environ. Sci. Technol.* **1971**, *5* (11), 1105−1112.
(68) Elimelech, M. Effect of Particle Size on the Kinetics of Particle Deposition under Attractive Double Layer Interactions. *J. Colloid Interface Sci.* **1994**, *164* (1), 190−199.
(69) Spiecker, P. M.; Gawrys, K. L.; Kilpatrick, P. K. Aggregation and Solubility Behavior of Asphaltenes and Their Subfractions. *J. Colloid Interface Sci.* **2003**, *267* (1), 178−193.

DOI: 10.1021/acs.energyfuels.8b03835
Energy Fuels 2019, 33, 1882−1891